THE JOURNAL OF BIOLOGICAL CHEMISTRY VOL. 281, NO. 4, pp. 1868–1875, January 27, 2006


# The Physical Properties of the Capsular Polysaccharides from *Cryptococcus neoformans* Suggest Features for Capsule Construction*

Received for publication, August 26, 2005, and in revised form, November 3, 2005 Published, JBC Papers in Press, November 8, 2005, DOI 10.1074/jbc.M509465200

**Diane C. McFadden**[‡1], **Magdia De Jesus**[§2], **and Arturo Casadevall**[‡§3]

*From the* [‡]*Department of Medicine, Division of Infectious Disease, and* [§]*Department of Microbiology and Immunology, Albert Einstein College of Medicine, Bronx, New York 10461*

**The most distinctive feature of the human pathogenic fungus is a polysaccharide capsule that is essential for virulence and is composed primarily of glucuronoxylomannan (GXM) and galactoxylomannan (GalXM). GXM mediates multiple deleterious effects on host immune function, yet relatively little is known about its physical properties. The average mass of *Cryptococcus neoformans* GXM from four antigenically different strains ranged from 1.7 to 7 × $10^6$ daltons as calculated from Zimm plots of light-scattering data. GalXM was significantly smaller than GXM, with an average mass of 1 × $10^5$ daltons. These molecular masses imply that GalXM is the most numerous polysaccharide in the capsule on a molar basis. The radius of gyration of the capsular polysaccharides ranged between 68 and 208 nm. Viscosity measurements suggest that neither polysaccharide altered fluid dynamics during infection since GXM behaved in solution as a polyelectrolyte and GalXM did not increase solution viscosity. Immunoblot analysis indicated heterogeneity within GXM. In agreement with this, scanning transmission electron microscopy of GXM preparations revealed a tangled network of two different types of molecules. Mass per length measurements from light scattering and scanning transmission electron microscopy were consistent and suggested GXM molecules self-associate. A mechanism for capsule growth is proposed based on the extracellular release and entanglement of GXM molecules.**

*Cryptococcus neoformans* causes life-threatening systemic disease in individuals with impaired immunity. Cryptococcosis is a relatively common disease in individuals with late stage human immunodeficiency virus disease, certain cancers, and transplanted organs (1). Recently, cases of cryptococcosis have been reported after anti- tumor necrosis factor-$\alpha$ therapy for rheumatoid arthritis (2–4), once again highlighting the potential of this organism to cause disease in immunosuppressed hosts. Suspected cryptococcal infection is often confirmed through microscopic identification of capsulated yeast from sputum or cerebrospinal fluid because *C. neoformans* is the only major fungal pathogen of humans that is encapsulated.

The polysaccharide capsule that surrounds the fungus promotes survival within the host (5). It is composed of two polysaccharides, glucuronoxylomannan (GXM)[4] and galactoxylomannan (GalXM). The capsule may also contain members of the large family of mannoproteins, which are present in the cell wall and are also secreted (6, 7). The vast majority of the capsular mass is thought to be GXM (~88%) (7), and this capsular component has, consequently, received most of the attention in immunological studies, which have consistently demonstrated numerous deleterious effects on immunological function. GXM inhibits phagocytosis of *C. neoformans* in the absence of opsonins and is either secreted or released from the organism into the surrounding tissue in large quantities (8, 9). GXM also inhibits a productive inflammatory response by disrupting macrophage maturation, neutrophil migration, and leukocyte extravasation while enhancing interleukin 10 production and down-regulating tumor necrosis factor-$\alpha$ and interleukin 1$\beta$ production (10–12). Although the mechanisms responsible for these effects are not well understood, GXM can interact with the cellular receptor CD14, and Toll-like receptors 2 and 4 (13). Binding of Toll-like receptor 4 appears critical for inhibiting neutrophil migration and the up-regulation of Fas ligand on macrophages (14, 15). GXM has attracted interest as a vaccine component and a target for antibody-based therapy since antibody to GXM is protective in animal models. Interestingly, the depressive effects of GXM on the immune system may imply usefulness as a therapeutic molecule capable of modulating the immune response in inflammatory diseases, such as streptococcal arthritis (16–20).

Knowledge on the structures and physical properties of GXM, GalXM, and the capsule is essential in understanding their role in cryptococcal pathogenesis and for the development of GXM-based therapeutic approaches. GXM is a co-polymer of up to six different repeating units that consists mostly of a linear $\alpha$(1→3)-mannan trisaccharide with side groups consisting of a $\beta$(1→2)-glucopyranosyluronic acid and 0–4 mol of $\beta$(1→2) and $\beta$(1→4)-xylopyranosyl (21).[5] The mannan backbone of GXM is modified by acetyl groups, although specific patterns of acetylation are unknown (22). The GXM of individual strains of *C. neoformans* differ in their ratios of the repeating units, and recent oligosaccharide compositional analysis suggests the occurrence of non-uniform side group addition and variability in co-polymerization (21).[5] Alterations in GXM composition have been experimentally correlated with changes in *C. neoformans* virulence, inhibition of neutrophil migration, and antibody recognition (15, 23–27).

In contrast to GXM, the contribution of GalXM to capsule architecture and pathogenesis has not been well studied. GalXM has an $\alpha$-(1,6)-galactan backbone containing four potential short oligosaccharide branch structures. The branches are 3-*O*-linked to the backbone and consist of an $\alpha$Man-(1→3)-$\alpha$Man (1→4)-$\beta$Gal trisaccharide with vari-

* This work was supported in part by National Institutes of Health Grants AI33774, AI33142, and HL59842–01 (to A. C.). The costs of publication of this article were defrayed in part by the payment of page charges. This article must therefore be hereby marked "*advertisement*" in accordance with 18 U.S.C. Section 1734 solely to indicate this fact.

[1] A Burroughs Wellcome Fund Fellow of the Life Science Research Foundation.
[2] Supported by NCI, National Institutes of Health Training Grant 2T32CA009173-31.
[3] To whom correspondence should be addressed: Albert Einstein College of Medicine, 1300 Morris Park Ave., Golding 701, Bronx, NY 10461. Tel.: 718-430-3665; Fax: 718-430-8701; E-mail: casadeva@aecom.yu.edu.

[4] The abbreviations used are: GXM, glucuronoxylomannan; GalXM, galactoxylomannan; $M_W$, weight-averaged mass; mAb, monoclonal antibody; STEM, scanning transmission electron microscopy.
[5] D. C. McFadden, F. Wang, and A. Casadevall, unpublished data.

able amounts of β(1→2) or β(1→3) xylose side groups (28). The backbone of GalXM consists of galactopyranose and a small amount of galactofuranose, unlike GXM, which only contains mannopyranose.

Studies of molecular mass revealed that GalXM is the more abundant polysaccharide in the capsule and that the mass of GXM from two var. *gatti* strains were larger than from two var. *neoformans* strains. Viscosity studies suggested that capsular polysaccharides do not disrupt normal fluid mechanics. Quantitative high resolution electron microscopy revealed two different GXM structures and, unexpectedly, suggested GXM self-interactions. A model of capsule assembly based upon polysaccharide-polysaccharide interactions is proposed.

## EXPERIMENTAL PROCEDURES

*GXM Isolation—C. neoformans* was grown in Sabouraud dextrose broth at 30 °C with shaking at 150 rpm. GXM was isolated from 2-week-old culture supernatant and purified as described by Cherniak *et al.* (21) with minor modifications. Supernatant was filtered through 0.45-μm filters to remove any cryptococcal cells remaining after low speed centrifugal separation. The polysaccharide was then precipitated from the supernatant with 10% (w/v) sodium acetate and 2.5 volumes of ethanol. The amount of carbohydrate in the water-solubilized precipitant was determined by the phenol-sulfuric acid method (29). The solution was adjusted to 0.2 M NaCl, and GXM was selectively precipitated using 3 g of hexyldecyltrimethylammonium bromide (Sigma) for each gram of carbohydrate present. GXM was then dissolved in 2 M NaCl, dialyzed extensively against 1 M NaCl to remove hexyldecyltrimethylammonium bromide, and then dialyzed against distilled water for 2 days. GXM was collected by lyophilization.

*GalXM Isolation*—GalXM was isolated from the culture supernatant according to Vaishnav *et al.* (28). Briefly, a 100-ml culture of *C. neoformans* acapsular mutant of strain B-3501, cap67, was grown in Sabouraud dextrose broth for 7 days. Although GalXM has been identified in the supernatant of a capsulated strain (7), the successful isolation of significant quantities of GalXM has been reported only for cap67. The use of this strain for GalXM production also prevented the contamination of the preparation with GXM, a complication present with capsulated strains. The culture supernatant was separated from the cells by centrifugation at 890 × *g* for 15 min at room temperature and then concentrated using a 10,000 $M_r$ cut-off Amicon centrifugal filter (Millipore, Bedford, MA). The material was then dialyzed for 3 days against distilled water, and the 10,000 retentate, containing GalXM and mannoproteins, was filter sterilized with a 0.2-μm filter. The solution was lyophilized and stored at room temperature. For separation of GalXM from the mannoproteins, the freeze-dried mixture was dissolved in 25 ml of start buffer. Start buffer consisted of a 0.01 M Tris base and 0.5 M NaCl solution, pH 7.2, to which $CaCl_2$ and $Mn(II)Cl_2$ was sequential added at final concentrations of 1 mM. The GalXM and mannoprotein solution was then continuously passed through a concanavalin A-Sepharose 4B column (2.5 × 10 cm) (Sigma) for 16 h at 4 °C using a peristaltic pump with a flow rate of 16 ml/h. The flow-through and 11 column washes of start buffer were collected as 20-ml fractions. GalXM-containing fractions, identified by a positive reaction in the phenol-sulfuric acid assay for carbohydrates (29), were combined, ultraconcentrated as before, and dialyzed against water for 7 days. GalXM was then recovered by lyophilization. Compositional analysis of GalXM was confirmed by combined gas chromatography/mass spectrometry of the per-*O*-trimethylsilyl derivatives of the monosaccharide methyl glycosides produced from the sample by acidic methanolysis.

*Molecular Mass Determination of GXM and GalXM*—The polysaccharides were diluted in sterile-filtered, degassed ultra-pure water to the desired concentrations from a freshly made 5 mg/ml stock solution. The change in refractive index (*dn/dc*) of the samples was measured by differential refractometry using a 620-nm laser source (BI-DNDC; Brookhaven Instruments Corp., Holtsville, NY) at 30 °C. The molecular mass was determined at room temperature by multi-angle laser light-scattering (BI-MwA analyzer, Brookhaven Instruments Corp., Holtsville, NY) using a 675-nm laser source. Before the mass measurements the system was calibrated against toluene and normalized for Rayleigh scattering with 20-nm microspheres (Duke Scientific Corp., Palo Alto, CA). The weight-averaged mass ($M_w$) was calculated by the Zimm equation (30), $Kc/\Delta R(\theta) = 1/(M_w)(P(\theta)) + 2A_2c$, where $K$ is the optical constant, defined as the quotient of $4\pi^2 n_o^2 (dn/dc)^2)/N_A \lambda_o^4$, and $\Delta R(\theta)$ is the excess Rayleigh factor, determined by comparing the sample and solvent values at angle ($\theta$) and concentration ($c$). $P(\theta)$ represents the particle scattering function, $A_2$ is the second virial coefficient, $n_o$ is the refractive index of the solvent, $N_A$ equals Avogadro's number, and $\lambda_o$ is the modal wavelength of the laser source. The *dn/dc* values were adjusted according to the Cauchy equation ($dn/dc = A + B/\lambda^2$), using a $B$ coefficient for aqueous solutions of +0.0022 μm and wavelengths ($\lambda$) in microns to accommodate for the longer wavelength of the molecular weight analyzer. Depolarization corrections were assumed to be negligible. All samples were passed through an in-line 0.8-μm syringe filter to eliminate large aggregates and reduce extraneous sources of refracted or scattered light.

*Electrophoretic Analysis of GXM*—A 0.5% (w/v) agarose solution was made by dissolving the agarose in 1× TAE buffer (40 mM Tris base, 20 mM sodium acetate, and 1 mM EDTA in ultrapure water) using microwave heating. The solution was not permitted to exceed the boiling point during the heating process and was cooled to 50 °C in a water bath before use. The agarose was poured into IBI/Shelton Scientific gel casting trays to produce either 70 × 100 × 6- or 200 × 250 × 6-mm gels. Sample wells were 2-mm wide. Gels were submerged in either 250 ml or 1.5 liters of 1× TAE buffer. GXM samples were 6 μl in volume and contained 10 μg of GXM and 1× loading buffer (30% glycerol, 0.25% bromphenol blue, 0.25% xylene cyanol FF). Electrophoresis conditions were 3 V/cm for 8 h.

Polysaccharide was transferred to Hybond Nylon$^+$ membrane (Amersham Biosciences) using a submerged tank blotting system (Genie Blotter; Idea Scientific, Minneapolis, MN). Transfer conditions were performed in 1× TAE at 9 V for 1 h. After transfer, the membrane was incubated for 30–60 min in 5% (w/v) nonfat milk in Tris-buffered saline (10 mM Tris, pH 7.2, 150 mM NaCl) followed by a standard Western blotting protocol. Primary antibodies used were murine monoclonal antibodies (mAbs) to GXM and are designated 2H1 (IgG1), 18B7 (IgG1), 12A1 (IgM), 13F1 (IgM), and 21D2 (IgM) (31–33). Primary antibodies were used at a concentration of 13 nM (2 μg/ml, IgG; 13.3 μg/ml, IgM). Secondary antibodies were either alkaline phosphatase-coupled goat-anti-mouse IgG1, -IgM, or -Igκ (Southern Biotechnology Associates, Birmingham, AL) and used at 1 μg/ml in Tris-buffered saline. GXM was visualized by incubating the membrane in the alkaline phosphatase detection substrates 5-bromo-4-chloro-3-indolyl phosphate/nitro blue tetrazolium (KPL, Gaithersburg, Maryland). At the completion of the reaction, the filters were rinsed briefly with distilled water and air-dried in the dark at room temperature.

*Capsule Thickness Measurements—C. neoformans* cells from 2-week-old cultures were suspended in India ink (BD Biosciences and visualized at 1000× magnification with an Olympus AX70 microscope. Images were captured with a QImaging Retiga 1300 digital camera using the QCapture Suite Version 2.46 software (QImaging, Burnaby BC,

Canada). Capsule measurements were made on 25 randomly chosen cells from each strain.

*Scanning Transmission Electron Microscopy*—GXM (1 mg) was dissolved in 1 ml of water over 3 days. The GXM solution was freeze-dried onto titanium electron microscope grids coated with a thick holey carbon film. Scanning transmission electron microscopy was performed at 40 keV with a 0.25-nm focused probe. Dark field images were digitally recorded as scans of 1.024 $\mu$m with a scanning pixel size of 20 Å$^2$. Mass measurements were calculated using the PCMass26 software. Tobacco mosaic virus was added to all samples as an internal control and had a mass per length of 131 kDa/nm.

*Viscosity*—Viscosity was measured using a modified Ostwald-type capillary glass viscometer (Cannon-Manning Semi-Micro, Technical Glass Co., Dover, NJ) at 25 °C. GXM and dextran (high fraction; East Kodak Co.) were dissolved in ultrapure water at a concentration of 10 mg/ml for 3–4 days at room temperature. GalXM was dissolved in ultrapure water at a concentration of 100 mg/ml for 2 days at room temperature. Diluted samples were made in ultrapure water, mixed, and equilibrated to 25 °C before testing. For intrinsic viscosity measurements, 3 ml of each sample was tested. For polyelectrolyte studies, 2.25 ml of each sample was tested. The ionic strength of the solution was adjusted with NaCl. Ionic strength was calculated by the standard equation $I = \frac{1}{2}\Sigma Z_i^2 C_i$, where $Z$ is the charge of the individual ions, and $C$ is the concentration of the individual ions. Flow-time measurements were taken in triplicate and averaged.

The relative viscosity increment ($\eta_i$; also known as specific viscosity, $\eta_{sp}$) is defined as the change in the ratio of the flow time of the sample to the solvent that is specifically due to the sample particles. The intrinsic viscosity ($[\eta]$) is defined as the limiting value of the reduced viscosity ($[\eta] = \lim_{c \to 0} (\eta_i/c)$). These terms and definitions are in accordance with the 1989 International Union of Pure and Applied Chemistry guidelines for polymers (34).

## RESULTS

*Average Molecular Mass and Radius of Gyration of Polysaccharides Determined from Multi-angle Laser Light Scattering*—The average molecular mass ($M_w$) of GXM from four genetically distinct strains was determined using multi-angle laser light scattering and the Zimm formalism (30). The different serotypes of *C. neoformans* have substantially different GXM structures, as determined by $^1$H NMR chemotyping analysis (21). Strains from the same serotype generally share significant similarities in their GXM structures (21). Therefore, the four strains also represented the four distinct serotypes (A, B, C, and D). The masses of GXM were derived from Zimm plots of light scattering data (Fig. 1). The $M_w$ of the examined GXMs (Table 1) ranged from 1.7 to 7.3 MDa. The smallest masses were for the GXMs from the var. *neoformans* strains; serotype A strain H99 followed by serotype D strain B-3501. The larger masses for GXM were from the *var. gatti* strains, with serotype C strain 106.97 larger than serotype B strain I23.

The radius of gyration ($R_g$) was also calculated from the light scattering data. The $R_g$ is the average distance between the center point of GXM to the outer edge of the molecule. The $R_g$ was determined in water and is the maximal length of the molecule, as the repulsive effect of the negative glucuronic acid sugars is maximized in the absence of counter ions. The $R_g$ values for the GXMs from the different strains showed substantial differences (68–208 nm) between strains (Table 1). The $R_g$ was used in conjunction with the $M_w$ to calculate the mass density of each GXM. Strain differences in mass density ranged from 17.22 to 67.65 kDa/nm (Table 1). Although $M_w$ appeared to correlate with varietal classification, $R_g$ did not show this trend, perhaps suggesting that the length of the molecule is a strain-specific characteristic of GXM.

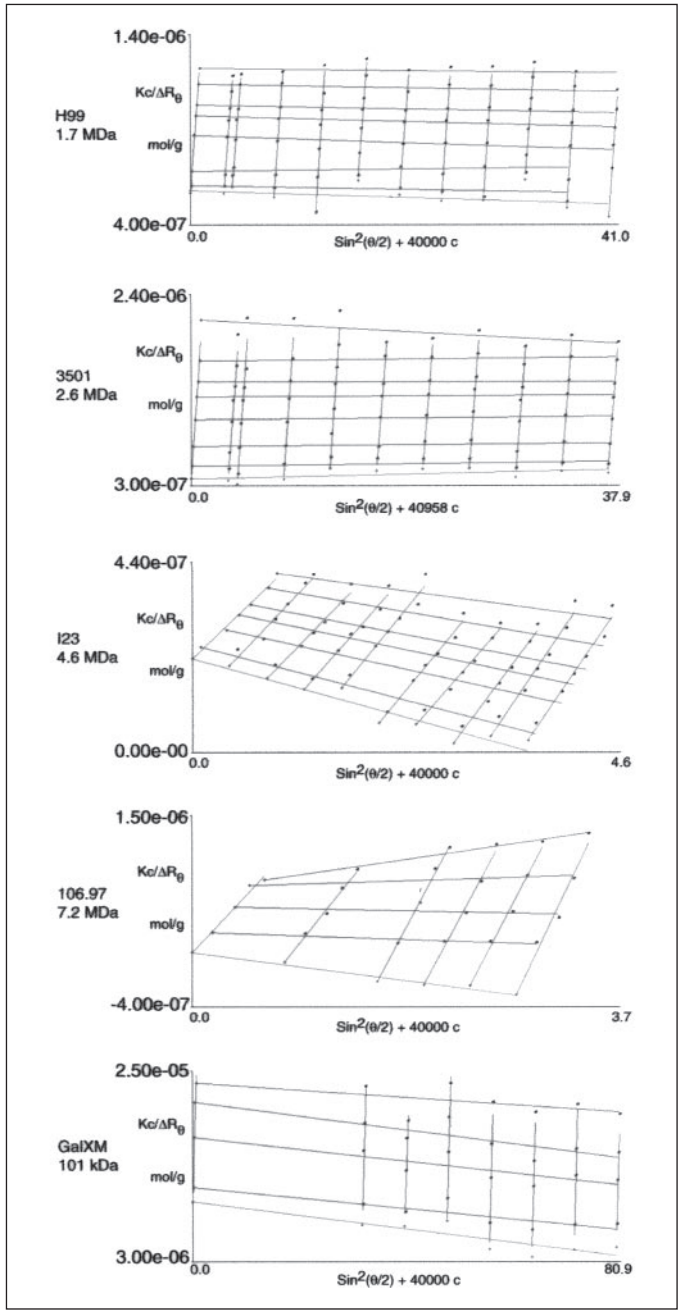


FIGURE 1. **Zimm plots of GXM from different strains of *C. neoformans* and GalXM from cap67.** The average molecular mass of each GXM was defined as the inverse of the *y* intercept for the derived lines for angle ($\theta$) approaches 0 and concentration ($c$) approaches 0. Strains and average molecular mass are listed to the *left* of the appropriate graph.

By light-scattering analysis, GalXM had an $M_w$ of 101,000 and an $R_g$ of 95 nm. The mass density, therefore, was 1.06 kDa/nm. The $M_w$ of GalXM from the acapsular mutant cap67 was 26-fold less than the $M_w$ of GXM from the parental strain B-3501. In contrast, the $R_g$ of the GalXM, which contains numerous small oligosaccharide branches, was only 1.4-fold smaller. Paired comparisons between GalXM and GXM from all strains were not possible since GalXM can only be isolated sufficiently from cultures lacking GXM, and acapsular variants of the other strains are unavailable.

**TABLE 1**

**Comparison of GXM composition, average mass ($M_W$), radius of gyration (Rg), mass density ($M_W$/Rg), capsule thickness ($\mu$m), dn/dc values, and second virial coefficients ($A_2$) for *C. neoformans* strains from four different serotypes**

N/A, not applicable. Cap67 lacks GXM and a recognizable capsule.

| Strain | Serotype | GXM composition[a] | Calculated mass of GXM repeat | $M_W$ | $R_g$ | $M_W/R_g$ | Capsule thickness | dn/*dc* (620 nm) | $A_2$ |
|---|---|---|---|---|---|---|---|---|---|
| | | | | $\times 10^6$ | *nm* | $\times 10^3$ | $\mu M$ | | $\times 10^{-3}$ *cm*$^3$ *mol/g*$^2$ |
| H99 | A | 12.7% M1, 57% M2, 15.7% M3, 2.3% M5, 12% M6[b] | 949.69 ± 63.55 | 1.7 ± 0.06 | 78 ± 2.8 | 21.79 | 0.6 ± 0.2 | 0.1602 | −0.01 ± 0.3 |
| B-3501 | D | 51% M1, 19% M2, 8% M5, 12% M6 | 867.70 | 2.6 ± 0.52 | 151 ± 20 | 17.22 | 0.5 ± 0.1 | 0.1532 | 0.06 ± 0.1 |
| I23 | B | 2% M1, 8.4% M2, 82% M3, 0.9% M4, 2.9% M5, 3.9% M6[c] | 1094.29 ± 42.76 | 4.6 ± 0.18 | 68 ± 3.4 | 67.65 | 1.7 ± 0.6 | 0.1549 | −1.18 ± 0.1 |
| 106.97 | C | 1.5% M1, 7.4% M2, 31.3% M3, 52.3% M4, 2.3% M5, 5.5% M6[d] | 1139.07 ± 112.92 | 7.2 ± 3.70 | 208 ± 65 | 34.62 | 2.0 ± 0.4 | 0.1549 | −3.01 ± 0.5 |
| Cap67 | D | GalXM | N/A | 0.101 ± 0.03 | 95 ± 24 | 1.06 | N/A | 0.1941 | −1.54 ± 0.5 |

[a] Cherniak *et al* (21).
[b] Average GXM composition and mass from 54 serotype A strains ± S.D.
[c] Average GXM composition and mass from 7 serotype B strains ± S.D.
[d] Average GXM composition and mass from 11 serotype C strains ± S.D.

A simplified measurement of molecular stiffness, or rigidity, suggested by Sist *et al.* (35) can be determined from the $M_w$ and $R_g$ data. The equation $R_g^2/N_w$, where $N_w$ is the number of sugar residues in the polysaccharide, was applied to the data for each strain. The data are: H99, 0.587 nm$^2$; B-3501, 1.609 nm$^2$; I23, 0.162 nm$^2$; 106.97, 0.941 nm$^2$.

*Polysaccharide Heterogeneity by Gel Electrophoresis*—Prior electrophoretic studies show that GXM exhibits minimal migration in SDS-polyacrylamide gels with high porosity (36, 37). In contrast, GalXM migrates within a 7% SDS-polyacrylamide gel (37). We reasoned that GXM was unable to migrate under SDS-PAGE conditions due to its ~10-fold larger mass. Therefore, electrophoretic analysis of the negatively charged GXM in 0.5% agarose gels was pursued. Attempts to visualize GXM directly in the agarose with carbohydrate stains were unsuccessful and complicated by the sugar-based nature of the agarose support matrix. After transfer to a positively charged nylon membrane, limited detection of GXM was achieved using 0.5% Alcian blue in 2% acetic acid (data not shown) (38). mAbs to GXM provided a sensitive means for polysaccharide detection (Fig. 2). The different antibodies used for immunodetection have different fine specificities (27), yet all recognized the same section of the immunoblot. This suggested that the material being detected is GXM and that entities exclusively recognized by a single mAb were not identifiable, possibly because each GXM molecule contained the multiple epitopes recognized by these antibodies. GXM was also transferred to nitrocellulose, and polyvinylidene difluoride membranes and mAbs detected the same area as on nylon membranes (data not shown). Variability in GXM detection on different lots of positively charged nylon was observed, although the areas of greatest GXM concentration were always detectable.

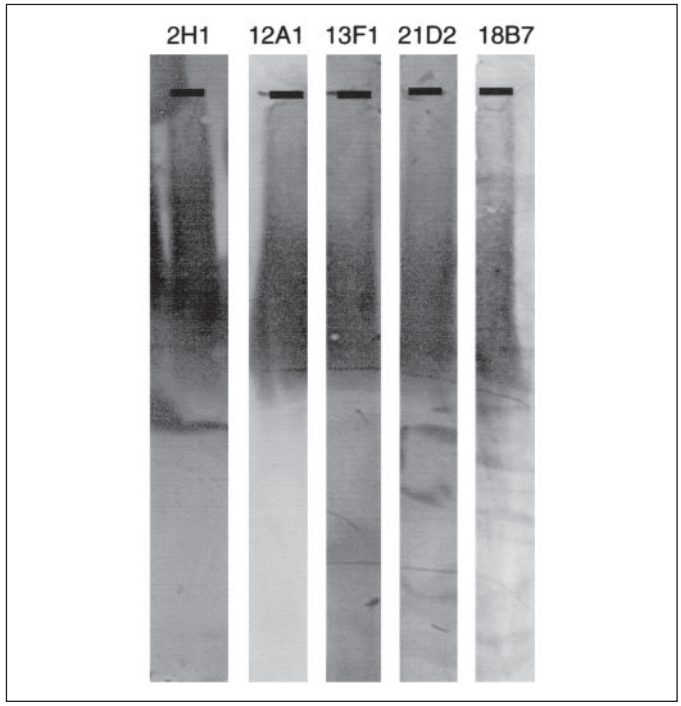


FIGURE 2. **Immunoblots of serotype D GXM from strain B-3501 with various mAbs.** mAbs 2H1 (IgG1), 18B7 (IgG1), 12A1 (IgM), an d 13F1 (1gM) were generated in response to serotype A GXM-conjugate (31). mAb 21D2 was generated in response to a murine *C. neoformans* infection with a clinical isolate (33). The *black line* represents the location of the sample well in the agarose gel.

The immunostaining of GXM revealed that the polysaccharide migrated over a significant area with some GXM still present near the sample well. Two potential explanations existed for this result. One was that GXM was heterogeneous, as is common for polysaccharides. The second was that the sample well had been overloaded. To distinguish between these possibilities, a lane of GXM, which had been subjected to electrophoresis, was cut from the gel and re-oriented horizontally at the top of a second agarose gel. The separated GXM formed the sample area of a second agarose gel and was subjected to a second round of electrophoresis. If the original migration pattern was an artifact of overloading, then by reducing the concentration of GXM at each point across the second gel a horizontal band of GXM should be detected by the antibodies. Instead, a diagonal migration pattern was observed after the second round of electrophoresis. The diagonal band could only be a result of individual structures of GXM migrating according to their individual electrophoretic properties (Fig. 3). Migration was unaltered by the inclusion of 0.1% SDS (data not shown) but was impaired with increasing concentrations of agarose (data not shown), suggesting that the separation of individual molecules was influenced by pore size and not charge. Therefore, GXM must be heterogeneous, and GXM molecules differ in their lengths or shapes.

*Scanning Transmission Electron Microscopy (STEM)*—STEM utilizes a high resolution microscope that images unstained molecules and has been used extensively to study large $M_w$ macromolecules, such as earthworm hemoglobin (39, 40). Because the images are unstained, the inten-

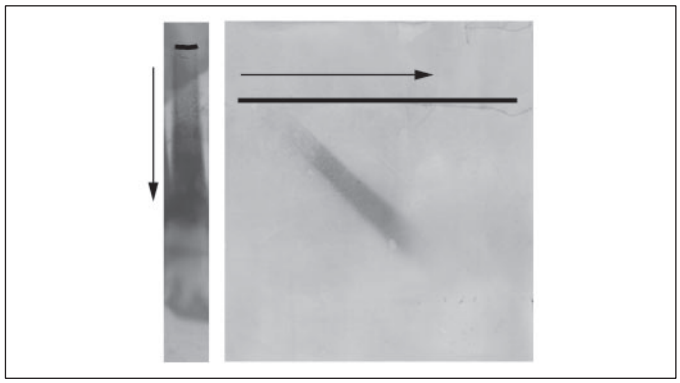

FIGURE 3. **GXM is composed of a heterogeneous population of molecules that can be electrophoretically separated.** *Left panel*, migration of 10 $\mu$g of GXM in a 0.5% agarose gel. *Right panel*, migration of GXM after a second round of electrophoresis. The sample lane was created by a 90° rotation of agarose containing previously electrophoresed GXM. The diagonal smear observed indicated that smearing was not an artifact of overloading but, rather, due to characteristically different electrophoretic properties within the polysaccharide. GXM is detected in both panels with mAb 2H1. GXM is detected in both panels with mAb 2H1 after transfer to nylon membrane. *Arrows* show migration of separated GXM after initial electrophoresis.

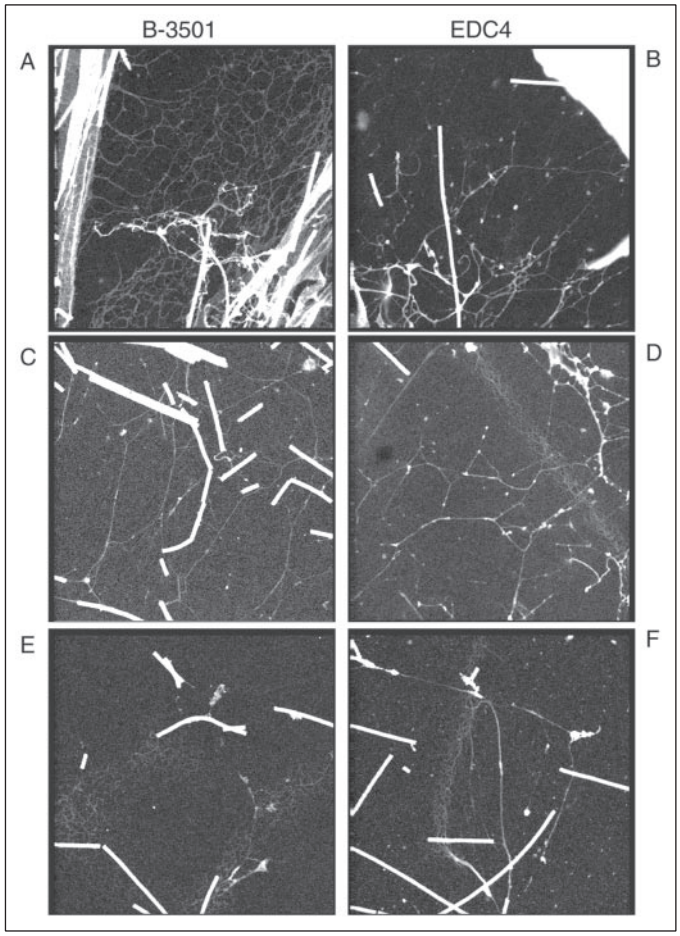


FIGURE 4. **STEM images of GXM from strain B-3501 (*left column*) and EDC4 (*right column*).** The internal control, tobacco mosaic virus, appears in each image as ***thick rods***. The GXM concentrations sampled for each image are as follows. *A*, 2 mg/ml; *B* and *D*, 320 $\mu$g/ml; *C*, 500 $\mu$g/ml; *E*, 100 $\mu$g/ml; *F*, 160 $\mu$g/ml.

sity of the scattered electrons can be used to quantitatively determine the mass of an object. Tobacco mosaic virus was included in all samples as an internal mass standard (131 kDa/nm).

High resolution images of unstained GXM obtained by STEM revealed intricate macromolecular structures. The predominant form

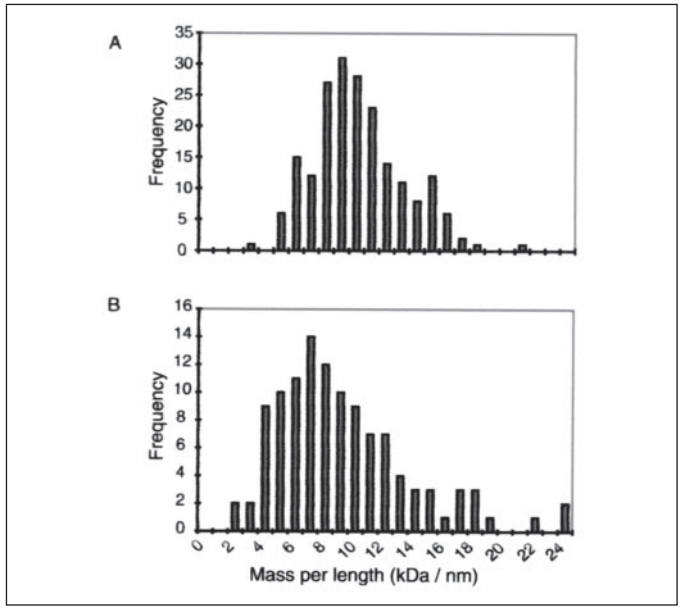


FIGURE 5. **Histograms showing the distribution of mass per length measurements for structure I fibers of GXM from strain B-3501 (*A*) and EDC4 (*B*).**

(Structure I) visible in the grids was composed of multiple long fibers entangled with one or more similar fibers (Fig. 4, *A* and *C*). Structure I fibers had an estimated average width of ~4 nm and an average mass per length of 10.63 ± 3.1 kDa/nm, which was normally distributed (Fig. 5*A*). The distribution was marginally skewed to the right (median mass per length of 10.26 kDa/nm) because of localized areas where fibers overlapped. The average mass per length derived from the STEM images closely approximated the average mass per length ($M_w/R_g$) calculated from the light scattering data, 17.6 kDa/nm, indicating internal consistency to these measurements. Because a disaccharide, within a polysaccharide, has a mass of 0.324 kDa and has an extended length of ~1 nm, then the mass density of Structure I implies that it is composed of multiple GXM molecules, which are possibly self-associating.

A second structure is also visible by STEM. This structure (Structure II) was composed of numerous small fibers extending in multiple directions (Fig. 4*E*). Because of the density of these fibers in a localized area and their lower signal intensities, width and mass per length measurements could not be determined by this technique.

Structures I and II were also visible in STEM images of isolated GXM from a capsular mutant of *C. neoformans*, EDC4 (27). The GXM from the mutant lacks the *O*-acetyl modification present in wild type strains. The structure I fibers of the mutant were also ~4 nm wide and normally distributed with an average mass per length (9.7 ± 4.4 kDa/nm) that is similar to wild type GXM (Fig. 5*B*). In addition, EDC4 GXM contained entangled structure I fibers and structure II fibers (Fig. 4, *B*, *D*, and *F*) (27). Therefore, the acetyl modification of GXM is not essential for the generation of these structures.

*Viscosity*—Intrinsic viscosity ([$\eta$]) measures the ability of a substance to increase the viscosity of a solution. The [$\eta$] of GXM from serotype C strain 106.97 in water was determined to be 840 $cm^3/g$.

The structural composition of GXM implies that it is an anionic polyelectrolyte. To determine whether GXM exhibited polyelectrolyte behavior in solution, the ionic strength of the solution was adjusted with NaCl, and the relative viscosity increment of the samples was measured. The relative viscosity increment of GXM decreased as the ionic strength of the solution was increased, suggesting that intramolecular electrostatic interactions between negatively charged glucuronic acids were

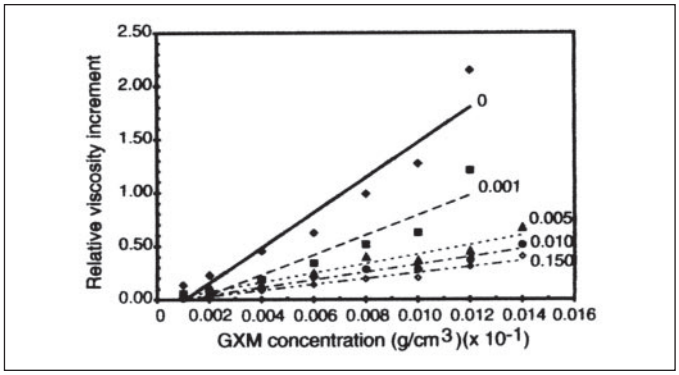


FIGURE 6. **GXM behaves as a polyelectrolyte in solution.** The relative viscosity increment decreases in response to an increase in the ionic strength of solution for GXM from strain 106.97. The ionic strength of the NaCl solution is listed to the *right* of the linear regression line for each concentration series.

disrupted by the sodium cations (Fig. 6). Ionic strength did not alter the relative viscosity increment of the uncharged control polysaccharide dextran (data not shown). Thus, GXM behaved in solution as a polyelectrolyte. GalXM did not significantly increase the viscosity of water at 7 mg/ml (69.3 $\mu$M; $\eta_i = 0.03$), despite the 5000-fold higher molar concentration when compared with GXM at 0.1 mg/ml (13.5 nM; $\eta_i = 0.14$)

## DISCUSSION

GXM and GalXM differed significantly in their molecular masses. The 17–74-fold difference between the negatively charged GXM and the smaller, uncharged GalXM has important implications for understanding the capsule architecture and also suggested that the $R_g$ of the polysaccharides should be quite different. The expectation of different sizes was supported by prior structural data indicating GalXM contained numerous branches of three to six sugars (28). Although GalXM was predicted to have a smaller $R_g$ than GXM, in fact the $R_g$ values were comparable. It is unclear to what extent GXM fiber entanglement may influence the average $R_g$ value since scenarios of molecular shortening and lengthening could occur. However, the $\alpha$-1,6 backbone of GalXM is inherently more flexible than the $\alpha$-1,3 backbone of GXM due to the presence of three bonds that are free to rotate in the glycosyl linkage instead of two. This major structural difference suggests that GalXM has a greater tendency toward a random coiled structure than GXM and, therefore, would have a more extended structure. Thus, the similarity in their $R_g$ values is probably a consequence of differences in their secondary structures.

The masses of GXM and GalXM were determined by light scattering. This approach avoided the use of assumptions regarding its hydrodynamic properties, such as the Stokes radius, viscosity, or derivation of the $M_w$ from a standard, which is particularly difficult for large polysaccharides. Serotype-dependent differences for GXM were identified. The $M_w$ for serotypes A and D averaged $2.2 \times 10^6$ and for serotypes B and C, $5.9 \times 10^6$. These $M_w$ values are larger than the mass of GXM originally estimated from hydrodynamic methods, $1–1.5 \times 10^6$ (41, 42). A few explanations exist for the $M_w$ differences. First, it is unclear if the earlier studies used GXM that was isolated after the autoclaving of cultures, a common practice in the past. The high temperatures used for autoclaving may have caused molecular breaks that lowered their $M_w$ relative to our samples. Second, the earlier studies employed hydrodynamic methods, namely diffusion, sedimentation, and size exclusion chromatography, where accurate resolution of a heterogeneous molecule is challenging and requires extrapolation to standards that correctly reflect the mass, structure, and hydrodynamic properties of the sample. Finding adequate standards for such studies is difficult given differences in branching, side groups, charge, and the different effects solvents have on their hydrodynamic properties, such as particle flow. Furthermore, the earlier data only examined var. *neoformans* strains, and our data demonstrate that the $M_w$ for var. *gatti* strains were larger than for var. *neoformans* strains.

Only a small portion of the large differences in the $M_w$ of GXM between var. *neoformans* and var. *gatti* strains are accountable by compositional differences in xylosylation (21). These differences were also not accountable for by the average length of GXM, as the $R_g$ values were independent of serotype. The differences in length and mass density between the GXM of individual strains, however, suggest differences in GXM conformation, as more compact polysaccharides generally have smaller $R_g$ values. Given that several biochemical differences between var. *neoformans* and var. *gatti* strains exist (43), the GXM $M_w$ differences are consistent with differences also being present in the synthetic machinery for GXM.

The $M_w$ of GalXM was more than half the value originally reported (101 *versus* 275 kDa) (7, 44). The capsule has been reported to contain a weight/weight ratio of GXM:GalXM and mannoprotein of 88:12 based on the total amount of material in culture supernatant (7). This led to the often-assumed conclusion that GXM is the most abundant molecule in the capsule. However, the large difference in molecular mass implies that the weight ratio derived from the supernatant does not reflect the relative abundance of each polysaccharide. The weight ratio can be used to determine the molar ratio of these polysaccharides in 1 g of capsular material. Assuming that the contribution of mannoprotein to the total polysaccharide mass is 5% or less, then for the B-3501 strain there are 2–3.5 mol of GalXM for each mol of GXM. If the exopolysaccharide composition and mass reflects that of capsular polysaccharide, then these results imply that there are more molecules of GalXM than GXM in the capsule. Therefore, GalXM is the major capsular polysaccharide on a molar basis. The lower quantity of GalXM in the supernatant may alternatively suggest that the polysaccharide is more tightly attached to the cell than GXM. This would be consistent with the reported immunolocalization of GalXM on the surface of an acapsular mutant (28) and the finding of galactose in capsular material obtained from the inner most layer of the capsule (45). Consequently, the larger molar amount of GalXM could suggest that the dense capsular material nearest to the cell wall under non-induced conditions is dominated by GalXM.

The large $M_w$ of GXM is reflected in its large [$\eta$]. The possibility that the viscosity of GXM had implications for pathogenesis was considered. Two aspects of cryptococcal infection where viscosity could be particularly relevant are the frequent lack of inflammatory cell infiltration in the lungs and the elevation of intracerebral pressure (46, 47). The decrease in GXM solution viscosity as ionic strength increased establishes that GXM behaves in solution as a polyelectrolyte. The reduction in viscosity is a consequence of cations neutralizing the repulsion between neighboring negative charges, which causes a change in the secondary structure. This behavior confirmed that the glucuronic acid sugars of GXM were solvent-exposed, as suggested by the precipitation of GXM by hexyldecyltrimethylammonium bromide. Because GXM exhibits polyelectrolyte behavior in solution, the high electrolyte concentrations present *in vivo* are predicted to relax the GXM conformation. Thus, although GXM in water was viscous, GXM in serum or cerebrospinal fluid is not predicted to impart significant viscosity to the fluids. GXM levels in serum and cerebrospinal fluid measured in rodent models are usually less than 100 $\mu$g/ml (46, 48, 49). At these concentrations viscosity should be low and unlikely to disrupt normal fluid dynamics in serum or central nervous system fluid. Therefore, GXM

probably does not create a physical barrier for the penetration of immune cells into the infection site nor inhibit the flow of blood or central nervous system fluid. GalXM did not increase the viscosity of water or salt solutions at high concentration and, therefore, also is unlikely to impair cellular movement. In situations where GXM or GalXM concentrations are much higher than normally observed, which has occasionally been detected in murine studies (50) and may occur intracellularly (51), viscosity effects may be applicable, although mouse sera containing as much as 1 mg/ml of GXM were not empirically observed to be viscous.

The highly entangled fibers of isolated GXM, visible by STEM, formed supra-structures reminiscent of the polysaccharide network observed in the capsule by freeze-fracture electron microscopy of whole cells (52, 53). This suggests that GXM in the capsule and exopolysaccharide preparations are similar. Hydrogen binding, hydrophobic effects, or cation bridges may be involved in the creation of these entangled fibers. Hydrogen bonding occurs in anhydrous preparations of the bacterial $\beta$-(1,3)-glucan curdlan (54), whereas bridges formed by $Ca^{2+}$ and other divalent cations cross-link anionic polysaccharide components of the plant cell wall component pectin (55). GXM migrated as a smear under electrophoretic conditions and was previously shown to elute as a broad peak during size exclusion chromatography, suggesting molecular heterogeneity within the polysaccharide (56). Although some of the heterogeneity may be due to length differences between GXM molecules, the STEM images indicated other sources of heterogeneity. Two different structures were observed, and each of them may have variability in their size. In addition, the entanglement of structure I fibers suggests structures with differences in total mass and overall shape are generated. The entangled fibers also suggest that the cross-linking apparent within the capsule is created by GXM and argues against a role of GalXM, the major capsular polysaccharide, or another minor component as a cross-linking molecule. The ultrastructure of GalXM remains unresolved. On an acapsular mutant, GalXM has been localized to the surface of the cell; however, currently, antibodies to GalXM, which could specifically identify it within the capsule matrix, are not available (28). Attempts to image GalXM by STEM were unsuccessful, possibly because the molecule may be too narrow to be detected, consistent with its low mass density.

The two different GXM structures identified by STEM were intriguing in light of recent evidence that different layers within the capsule matrix are chemically distinguishable (45, 57). Structure I was most similar to the capsule architecture evident in electron microscopy of intact cells. However, the presence of structure II in wild type and de-*O*-acetylated GXM suggests that it also may be important in capsule formation. Isolated GXM adheres to the surface of an acapsular *C. neoformans* strain and forms a thin polysaccharide coating. This coating is sufficient to inhibit macrophage phagocytosis, a capsule-associated property (8), but does not resemble a wild type capsule. In fact, the number of GXM molecules that attaches is ~73-fold less than the number calculated to be on the surface of a capsulated cell (45, 58). A possible explanation for this is that the assembly of structures I and II into a capsule does not occur under the *in vitro* conditions.

The average mass of structure I GXM fibers in a given length is normally distributed, suggesting that a basic structural unit exists. Molecular models of GXM predict a 2- or 3-fold helical structure (22). X-ray diffraction analysis of an $\alpha(1\rightarrow3)$ mannan from a non-*Cryptococcus* Basidiomycetes also predicts a 2-fold structure (22, 59). Achieving a mass per length that is ~10 kDa/nm cannot be accommodated by a simple 2- or 3-fold structure. Therefore, the data suggest that the fibers are composed of multiple GXM molecules, perhaps forming a bundle-like structure. The flexibility or rigidity, which influences the persistence length of the GXM structure in solution, is affected by the combination of different factors, such as ionic strength, the surface exposure of negative charges, and the number of fibers within the structure. Calculations of the rigidity based on the method of Sist *et al.* (35) suggest GXM is a flexible polymer in solution.

The physical and structural data on GXM provide new information for inclusion into the current concept of capsule assembly and growth. The variability in the $R_g$ and mass density of GXM from the different strains suggest differences in GXM conformation and may imply architectural differences in the assembled capsules. The capsule of *C. neoformans* undergoes a dramatic alteration in size during pathogenesis and is regulated by environmental and nutrient cues (60, 61). The capsule thickness of the strains studied ranged from 0.5 to 2.0 $\mu$m, whereas their $R_g$ values ranged from 68 to 208 nm. Therefore, a single molecule of GXM cannot span the distance from the cell wall to the capsule edge. Consequently, the construction and expansion of the capsule must include the production of GXM fibers that are released from and not attached to the cell. The intracellular synthesis of GXM may include the formation of structure I-like fibers. Qualitatively, these fibers appear to dominate the capsule and the GXM exopolysaccharide. Monoclonal antibodies to GXM that recognize the capsule and the exopolysaccharide also bind an antigen in intracellular vesicles within the yeast (31, 62–66). This antigen is presumably GXM. For specific antibody binding to occur, the synthesis of intracellular GXM likely results in the formation of some of the same structures as exist in extracellular GXM. Assuming that capsular material is delivered to the capsule in vesicles (62, 66), changes in the capsule can occur by newly synthesized GXM fibers being released and incorporated throughout the capsule by becoming entangled in existing capsular material. The density gradient of capsular material provides for more points of contact at the inner layer than at the outer layer with other existing GXM fibers (57). Capsule assembly and growth would, therefore, be a consequence of a concentration-dependent self-associative process and infers that the primary GXM structure encodes the necessary information for capsule construction. GXM fibers that failed to find a suitable attachment point would be, by default, released as exopolysaccharide. This assumes that the exopolysaccharide is representative of polysaccharide retained in the capsule. Indeed, monoclonal antibodies to GXM recognize cell-associated GXM and exopolysaccharide (31, 63), and the ultrastructure visible in freeze-fracture images of the capsule (53) and STEM images of exopolysaccharide are similar in appearance, suggesting structural relatedness. Furthermore, the capsule contracts in response to the presence of salt (57, 67), as expected given the viscoelastic properties demonstrated in this work of a polyelectrolyte molecule. The overlapping of individual polysaccharide molecules to expand the thickness of the capsule may involve either an increase in GXM production or the synthesis of GXM polymers with a higher attraction to existing fibers.

Cell biology studies of capsule synthesis have suggested that new capsule material is added near the cell wall, leading to a greater density in capsular material in this region, and pushes older material outwards (53). More recently, antibody penetration studies have suggested that capsular regions more distal from the cell wall also have an increased density in enlarged capsules, and capsule phenotype studies have suggested the formation of a new GXM structure at the periphery of the capsule (24, 57). Although the data presented cannot distinguish between different modes of capsule growth, a capsule construction model dependent on the self-association of GXM does unify several observations. The increase in capsular material could be explained by the concentration-dependent addition of new GXM fibers throughout

the capsule; the cross-linking, porosity gradient, and proposed remodeling of the capsule could be an outcome of entanglement., and the association of new GXM with existing fibers near the capsule periphery or structural changes in the capsule due to the cross-linking of polysaccharide might generate new antigenic structures at the edge of the capsule (24, 53, 57).

*Acknowledgments—We thank Dr. Thomas Mitchell, Duke University, and Dr. Uma Banerjee, All India Institute of Medical Sciences, for providing strains 106.97 and I23, respectively. We thank Dr. Robert Cherniak, University of Georgia, for sharing unpublished data on the GXM composition of different strains. We thank Joseph Wall and Martha Simon at Brookhaven National Laboratories for the STEM images. The Brookhaven National Laboratories STEM is a National Institutes of Health Supported Resource Center, NIH 5 P41 EB2181, with additional support provided by the Department of Energy, Office of Biological and Environmental Research. We thank the Complex Carbohydrate Research Center at The University of Georgia for GalXM composition analysis. The Complex Carbohydrate Research Center is supported by the Department of Energy Center for Plant and Microbial Complex Carbohydrates, DE-FG09-93ER-20097. We also thank Bettina Fries and Oscar Zaragoza for critical reading of the manuscript.*

## REFERENCES


1. Perfect, J. R., and Casadevall, A. (2002) *Infect. Dis. Clin. North Am.* **16,** 837–874, 5–6
2. Arend, S. M., Kuijper, E. J., Allaart, C. F., Muller, W. H., and Van Dissel, J. T. (2004) *Eur. J. Clin. Microbiol. Infect. Dis.* **23,** 638–641
3. Shrestha, R. K., Stoller, J. K., Honari, G., Procop, G. W., and Gordon, S. M. (2004) *Respir. Care* **49,** 606–608
4. Hage, C. A., Wood, K. L., Winer-Muram, H. T., Wilson, S. J., Sarosi, G., and Knox, K. S. (2003) *Chest* **124,** 2395–2397
5. Kozel, T. R., and Cazin, J., Jr. (1971) *Infect. Immun.* **3,** 287–294
6. Vartivarian, S. E., Reyes, G. H., Jacobson, E. S., James, P. G., Cherniak, R., Mumaw, V. R., and Tingler, M. J. (1989) *J. Bacteriol.* **171,** 6850–6852
7. Cherniak, R., Reiss, E., and Turner, S. H. (1982) *Carbohydr. Res.* **103,** 239–250
8. Kozel, T. R. (1977) *Infect. Immun.* **16,** 99–106
9. Casadevall, A., Mukherjee, J., and Scharff, M. D. (1992) *J. Immunol. Methods* **154,** 27–35
10. Vecchiarelli, A., Pietrella, D., Lupo, P., Bistoni, F., McFadden, D. C., and Casadevall, A. (2003) *J. Leukocyte Biol.* **74,** 370–378
11. Vecchiarelli, A., Retini, C., Pietrella, D., Monari, C., Tascini, C., Beccari, T., and Kozel, T. R. (1995) *Infect. Immun.* **63,** 2919–2923
12. Monari, C., Bistoni, F., Casadevall, A., Pericolini, E., Pietrella, D., Kozel, T. R., and Vecchiarelli, A. (2005) *J. Infect. Dis.* **191,** 127–137
13. Shoham, S., Huang, C., Chen, J. M., Golenbock, D. T., and Levitz, S. M. (2001) *J. Immunol.* **166,** 4620–4626
14. Monari, C., Pericolini, E., Bistoni, G., Casadevall, A., Kozel, T. R., and Vecchiarelli, A. (2005) *J. Immunol.* **174,** 3461–3468
15. Ellerbroek, P. M., Lefeber, D. J., van Veghel, R., Scharringa, J., Brouwer, E., Gerwig, G. J., Janbon, G., Hoepelman, A. I., and Coenjaerts, F. E. (2004) *J. Immunol.* **173,** 7513–7520
16. Mukherjee, S., Lee, S., Mukherjee, J., Scharff, M. D., and Casadevall, A. (1994) *Infect. Immun.* **62,** 1079–1088
17. Feldmesser, M., and Casadevall, A. (1998) *Front. Biosci.* **3,** 136–151
18. Devi, S. J., Schneerson, R., Egan, W., Ulrich, T. J., Bryla, D., Robbins, J. B., and Bennett, J. E. (1991) *Infect. Immun.* **59,** 3700–3707
19. Pirofski, L. A. (2001) *Trends Microbiol* **9,** 445–451
20. Tissi, L., Puliti, M., Bistoni, F., Mosci, P., Kozel, T. R., and Vecchiarelli, A. (2004) *Infect. Immun.* **72,** 6367–6372
21. Cherniak, R., Valafar, H., Morris, L. C., and Valafar, F. (1998) *Clin. Diagn. Lab. Immunol.* **5,** 146–159
22. Cherniak, R., Jones, R. G., and Reiss, E. (1988) *Carbohydr. Res.* **172,** 113–138
23. Cleare, W., Cherniak, R., and Casadevall, A. (1999) *Infect. Immun.* **67,** 3096–3107
24. Charlier, C., Chretien, F., Baudrimont, M., Mordelet, E., Lortholary, O., and Dromer, F. (2005) *Am. J. Pathol.* **166,** 421–432
25. Janbon, G., Himmelreich, U., Moyrand, F., Improvisi, L., and Dromer, F. (2001) *Mol. Microbiol.* **42,** 453–467
26. Fries, B. C., Goldman, D. L., Cherniak, R., Ju, R., and Casadevall, A. (1999) *Infect. Immun.* **67,** 6076–6083
27. McFadden, D. C., and Casadevall, A. (2004) *J. Immunol.* **172,** 3670–3677
28. Vaishnav, V. V., Bacon, B. E., O'Neill, M., and Cherniak, R. (1998) *Carbohydr. Res.* **306,** 315–330
29. Dubois, M., Gilles, K. A., Hamilton, J. K., Rebers, P. A., and Smith, F. (1956) *Anal. Chem.* **28,** 350–356
30. Zimm, B. H. (1948) *J. Chem. Phys.* **16,** 1093–1099
31. Casadevall, A., Mukherjee, J., Devi, S. J., Schneerson, R., Robbins, J. B., and Scharff, M. D. (1992) *J. Infect. Dis.* **165,** 1086–1093
32. Mukherjee, J., Casadevall, A., and Scharff, M. D. (1993) *J. Exp. Med.* **177,** 1105–1116
33. Casadevall, A., and Scharff, M. D. (1991) *J. Exp. Med.* **174,** 151–160
34. Kratochvil, P., and Suter, U. W. (1989) *Pure Appl. Chem.* **61,** 211–241
35. Sist, P., Cescutti, P., Skerlavaj, S., Urbani, R., Leitao, J. H., Sa-Correia, I., and Rizzo, R. (2003) *Carbohydr. Res.* **338,** 1861–1867
36. Murphy, J. W., and Pahlavan, N. (1979) *Infect. Immun.* **25,** 284–292
37. Murphy, J. W., Mosley, R. L., Cherniak, R., Reyes, G. H., Kozel, T. R., and Reiss, E. (1988) *Infect. Immun.* **56,** 424–431
38. Lee, H. G., and Cowman, M. K. (1994) *Anal. Biochem.* **219,** 278–287
39. Martin, P. D., Kuchumov, A. R., Green, B. N., Oliver, R. W., Braswell, E. H., Wall, J. S., and Vinogradov, S. N. (1996) *J. Mol. Biol.* **255,** 154–169
40. Thomas, D., Schultz, P., Steven, A. C., and Wall, J. S. (1994) *Biol. Cell* **80,** 181–192
41. Gadebusch, H. H., Ward, P. A., and Frenkel, E. P. (1964) *J. Infect. Dis.* **114,** 95–106
42. Turner, S. H., and Cherniak, R. (1991) *Carbohydr. Res.* **211,** 103–116
43. de Hoog, G. S., Guarro, J., Gene, J., and Figueras, M. J. (2000) *Atlas of Clinical Fungi*, 2nd Ed., pp. 130–143, Universitat Rovira i Virgili, Reus
44. James, P. G., and Cherniak, R. (1992) *Infect. Immun.* **60,** 1084–1088
45. Bryan, R. A., Zaragoza, O., Zhang, T., Ortiz, G., Casadevall, A., and Dadachova, E. (2005) *Eukaryot. Cell* **4,** 465–475
46. Fries, B. C., Lee, S. C., Kennan, R., Zhao, W., Casadevall, A., and Goldman, D. L. (2005) *Infect. Immun.* **73,** 1779–1787
47. Goldman, D. L., Fries, B. C., Franzot, S. P., Montella, L., and Casadevall, A. (1998) *Proc. Natl. Acad. Sci. U. S. A.* **95,** 14967–14972
48. Feldmesser, M., and Casadevall, A. (1997) *J. Immunol.* **158,** 790–799
49. Dromer, F., Charreire, J., Contrepois, A., Carbon, C., and Yeni, P. (1987) *Infect. Immun.* **55,** 749–752
50. Taborda, C. P., and Casadevall, A. (2001) *J. Immunol.* **166,** 2100–2107
51. Feldmesser, M., Kress, Y., Novikoff, P., and Casadevall, A. (2000) *Infect. Immun.* **68,** 4225–4237
52. Sakaguchi, N. (1993) *Virchows Arch. B Cell Pathol.* **64,** 57–66
53. Pierini, L. M., and Doering, T. L. (2001) *Mol. Microbiol.* **41,** 105–115
54. McIntosh, M., Stone, B. A., and Stanisich, V. A. (2005) *Appl. Microbiol. Biotechnol.* **68,** 163–173
55. Vincken, J. P., Schols, H. A., Oomen, R. J., McCann, M. C., Ulvskov, P., Voragen, A. G., and Visser, R. G. (2003) *Plant Physiol.* **132,** 1781–1789
56. Fries, B. C., Taborda, C. P., Serfass, E., and Casadevall, A. (2001) *J. Clin. Investig.* **108,** 1639–1648
57. Gates, M. A., Thorkildson, P., and Kozel, T. R. (2004) *Mol. Microbiol.* **52,** 13–24
58. Kozel, T. R., and Hermerath, C. A. (1984) *Infect. Immun.* **43,** 879–886
59. Ogawa, K., Miyanishi, T., Yui, T., Hara, C., Kiho, T., Ukai, S., and Sarko, A. (1986) *Carbohydr. Res.* **148,** 115–120
60. Rivera, J., Feldmesser, M., Cammer, M., and Casadevall, A. (1998) *Infect. Immun.* **66,** 5027–5030
61. Janbon, G. (2004) *FEMS Yeast Res* **4,** 765–771
62. Feldmesser, M., Kress, Y., and Casadevall, A. (2001) *Microbiology* **147,** 2355–2365
63. Nussbaum, G., Cleare, W., Casadevall, A., Scharff, M. D., and Valadon, P. (1997) *J. Exp. Med.* **185,** 685–694
64. Cleare, W., Mukherjee, S., Spitzer, E. D., and Casadevall, A. (1994) *Clin. Diagn. Lab. Immunol.* **1,** 737–740
65. Lendvai, N., Casadevall, A., Liang, Z., Goldman, D. L., Mukherjee, J., and Zuckier, L. (1998) *J. Infect. Dis.* **177,** 1647–1659
66. Garcia-Rivera, J., Chang, Y. C., Kwon-Chung, K. J., and Casadevall, A. (2004) *Eukaryot. Cell* **3,** 385–392
67. Jacobson, E. S., Tingler, M. J., and Quynn, P. L. (1989) *Mycoses* **32,** 14–23